

# Field comparison of two novel open-path instruments that measure dry deposition and emission of ammonia using flux-gradient and eddy covariance methods

5 Daan Swart<sup>1</sup>, Jun Zhang<sup>2</sup>, Shelley van der Graaf<sup>1</sup>, Susanna Rutledge-Jonker<sup>1\*</sup>, Arjan Hensen<sup>2</sup>, Stijn Berkhout<sup>1</sup>, Pascal Wintjen<sup>2,4</sup>, René van der Hoff<sup>1</sup>, Marty Haaima<sup>1</sup>, Arnoud Frumau<sup>2</sup>, Pim van den Bulk<sup>2</sup>, Ruben Schulte<sup>1,3</sup>, Margreet van Zanten<sup>1</sup>, Thomas van Goethem<sup>1</sup>

<sup>1</sup> National Institute for Public Health and the Environment (RIVM), P.O. Box 1, 3720 BA, Bilthoven, the Netherlands

10 <sup>2</sup> Netherlands Organisation for Applied Scientific Research (TNO), P.O. Box 15, 1755 ZG, Petten, the Netherlands

<sup>3</sup> Wageningen University & Research (WUR), P.O. Box 47, 6700 AA, Wageningen, the Netherlands

<sup>4</sup> Thünen Institute of Climate-Smart Agriculture, Bundesallee 68, 38116 Braunschweig, Germany

\*Correspondence to: susanna.jonker@rivm.nl

15 **Abstract.** Dry deposition of ammonia (NH<sub>3</sub>) is the largest contributor to the nitrogen deposition from the atmosphere to soil and vegetation in the Netherlands, causing eutrophication and loss of biodiversity. Yet, data sets of NH<sub>3</sub> fluxes are sparse and in general have monthly resolution at best. An important reason for this is that measurement of the NH<sub>3</sub> flux under dry conditions is notoriously difficult. There is no technique that can be considered as the golden standard for these measurements, which complicates the testing of new techniques. Here, we present the results of an intercomparison of two novel measurement  
20 setups aimed at measuring dry deposition of NH<sub>3</sub> at half-hourly resolution. In a five-week period, we operated two novel optical open-path techniques side by side at the Ruisdael station in Cabauw, the Netherlands: the RIVM-miniDOAS 2.2D using the aerodynamic gradient technique, and the commercial Healthy Photon HT8700E using the eddy covariance technique. These instruments are widely different in their measurement principle and approach to derive deposition values from measured concentrations. Yet, both techniques showed very similar results ( $r = 0.87$ ) and small differences in cumulative fluxes (~10%)  
25 as long as the upwind terrain was homogeneous and free of nearby obstacles. The observed fluxes varied from ~ -80 to ~ +140 ng NH<sub>3</sub> m<sup>-2</sup> s<sup>-1</sup>. Both the absolute flux values and the temporal patterns were highly similar, which substantiates that both instruments were able to measure NH<sub>3</sub> fluxes at high temporal resolution. However, for wind directions with obstacles nearby, the correlations between the two techniques were weaker. The uptime of the miniDOAS system reached 100% once operational, but regular intercalibration of the system was applied in this campaign (35% of the 7-week uptime). Conversely,  
30 the HT8700E did not measure during, and shortly after, rain, and the coating of its mirrors tended to degrade (21% data loss during the 5-week uptime). In addition, the NH<sub>3</sub> concentrations measured by the HT8700E proved sensitive to air temperature, causing substantial differences (range: -15 to + 6 μg m<sup>-3</sup>) between the two systems. To conclude, the miniDOAS system appears ready for long-term hands-off monitoring. The current HT8700E system, on the other hand, had a limited stand-alone operational time under the prevailing weather conditions. However, under relatively dry and low-dust conditions, the system  
35 can provide sound results, opening good prospects for future versions, also for monitoring applications. The new high temporal resolution data from these instruments can facilitate the study of processes behind NH<sub>3</sub> dry deposition, allowing an improved understanding of these processes and better parametrization in chemical transport models.

## 1 Introduction

Human alteration of the global nitrogen cycle through agricultural, industrial, and combustion processes has led to  
40 unprecedented levels of reactive nitrogen (N<sub>r</sub>) in the Earth system (Galloway et al., 2021; Fowler et al., 2013). Besides benefits like increased food production, losses of N<sub>r</sub> have a range of detrimental effects on both the environment and human health

(Sutton et al., 2011; Erisman et al., 2015). Gaseous  $\text{NH}_3$  can be emitted from and deposited onto the Earth's surface: the exchange is bi-directional. With regards to deposition, dry deposition of  $\text{NH}_3$  is an important component. In the Netherlands for example, it typically accounts for more than a third of the total  $\text{N}_r$  deposition (Hoogerbrugge et al., 2020). Accurate  
45 quantification of biosphere-atmosphere exchange of  $\text{NH}_3$  is therefore essential to increase our understanding of  $\text{NH}_3$  budgets at regional and global scales, to study relevant processes at high time resolution, monitor trends, measure the effectiveness of mitigation efforts, and improve and validate air quality and deposition models.

Despite the relevance of high-quality measurements of  $\text{NH}_3$  exchange, relatively few direct long-term continuous measurements have been reported. Dry deposition of  $\text{NH}_3$  can be highly variable in time and space and depends on a variety  
50 of site-specific parameters like canopy wetness, leaf area, and surface roughness (Flechard et al., 2011). Micro-meteorological techniques provide the most direct estimates of dry deposition, but these measurements each present their technical challenges and generally require substantial expense and labour.

The aerodynamic flux gradient method (AGM, also 'profile method') has delivered the majority of the  $\text{NH}_3$  dry deposition data worldwide. Most of these measurements were done using wet chemical instrumentation (e.g. Erisman and Wyers, 1993;  
55 Loubet et al., 2012), but nowadays also optical  $\text{NH}_3$  measurement systems are used (e.g. Kamp et al., 2020). In the AGM method, surface-atmosphere exchange fluxes are derived from measurements of vertical concentration differences ( $d_{\text{NH}_3}$ ) combined with a measure of vertical turbulent transport (Loubet and Personne, 2016; Prueger and Kustas, 2005). Drawbacks of AGM (listed by Trebs et al., 2021; Loubet et al., 2013) include potentially biased gradients under non-stationary conditions if sequential sampling at multiple heights using one monitor is required (Kamp et al., 2020), or, if using multiple monitors, the  
60 need for regular side-by-side comparisons to accurately determine and correct for any potential systematic difference (bias) between monitors (Wolff et al., 2010; Walker et al., 2013). Finally, a drawback of AGM is the need to rely on empirical stability corrections, which are based on relationships found for sensible heat, but assumed to be the same for trace compounds like  $\text{NH}_3$ .

Open-path (OP) techniques avoids the delay effects, reduced temporal resolution and interference from aerosols that result  
65 from  $\text{NH}_3$  sticking to inlet lines, air filters and other surfaces in an instrument (Parrish and Fehsenfeld, 2000). OP analysers have no sampling tubes and provide a way of measuring concentration in situ, without interfering with the airflow. A long-line averaging open-path gas analyser allows measurements of path integrated  $\text{NH}_3$  concentrations at a high time resolution. Optical analysers now available include those based on Fourier Transform Infrared (FTIR) (Sintermann et al., 2011; Flesch et al., 2016), tuneable diode laser TDL (Bai et al., 2022) or differential optical absorption DOAS spectroscopy (Volten et al.,  
70 2012b; Sintermann et al., 2016). These instruments can be used to measure the difference in  $\text{NH}_3$  concentration between two vertically offset paths, either in slant configuration (e.g. Bai et al., 2021; Flesch et al., 2016) or in two parallel horizontal paths. In the Netherlands, several experiments have taken place using two DOAS systems to measure  $d_{\text{NH}_3}$  (Wichink Kruit et al., 2010; Volten et al., 2012a; Schulte et al., 2020). Over the last year, the more recently developed miniDOAS (Berkhout et al., 2017) has been adapted and improved to meet the high sensitivity required for flux gradient measurements of  $\text{NH}_3$  (Wolff et al.,  
75 al., 2010; Foken, 2017).

Eddy covariance (EC) is the preferable technique for measuring the surface-atmosphere gas exchange of any compound because it provides the most direct measurement. However, EC requires fast ( $<0.1$  s) and precise concentration measurements, which is particularly challenging for  $\text{NH}_3$ . In recent years, several studies have reported measurements of the  $\text{NH}_3$  flux using closed-path (CP) analysers (Famulari et al., 2004; Moravek et al., 2019; Zöll et al., 2016). However, the reactivity and solubility  
80 of  $\text{NH}_3$  in water presents challenges there, because the use of inlet tubing leads to loss of fast variations in the signal.

So far, two folded-path open-path instruments are available for eddy covariance measurements of  $\text{NH}_3$ . Besides the benefit compared to the CP setup of not needing an inlet tube, such systems generally have much lower power requirements and the less bulky installation may allow for a more portable and adaptable setup also at more remote sites.

The first OP EC NH<sub>3</sub> analyser is the QCL-based instrument developed by Princeton University, and improved from the original design presented in Miller et al. (2014) over various deployments (Sun et al., 2015; Pan et al., 2021). More recently, a similar instrument has become available from Healthy Photon Co. Ltd., Ningbo, China: model HT8700 (Wang et al., 2021). Limitations of open-path EC flux measurements include interference from contamination by dust and rainfall, and the influence of exposure of the instrument to outdoor conditions. Since this technique is evaluating the net flux by measuring concentration levels in both up and down going air that passes the sensing volume both in small, high frequency (> 5 Hz) eddies and in slow (> 10 minute) large turbulent eddies the method needs corrections for differences in air density between up and down going air. Similar to closed-path EC gas analysers, not all sizes and frequencies of eddies are measured completely and therefore (high and low frequency) spectral corrections are needed.

Both micrometeorological methods (AGM and EC) share additional limitations to those mentioned above, such as the need for a homogeneous upwind fetch to avoid local advection errors. They also require steady-state conditions, well-developed turbulence, with no change in vertical flux with height (Loubet et al., 2013; Mauder et al., 2021).

In this study, we measured bi-directional NH<sub>3</sub> fluxes in a field campaign of seven weeks from August 24<sup>th</sup> to October 11<sup>th</sup>, 2021 over grassland at the Cabauw research site in the Netherlands, during which both deposition and emission events were encountered. During a period of 5 weeks (August 27<sup>th</sup> to October 1<sup>st</sup>), we compared measurements of NH<sub>3</sub> concentrations and fluxes from two open-path instruments: the RIVM miniDOAS 2.2D using the AGM, and the commercial HT8700E from Healthy Photon Inc. using the EC technique. This was the first time either one of these systems was compared to another setup. The primary aim of the campaign was to test if both novel instruments were indeed capable of measuring the dry exchange flux of NH<sub>3</sub> at high temporal resolution. Here, we describe the uptime and performance of both setups and compared the results of both concentration and flux measurements of NH<sub>3</sub>. Moreover, potential sources of errors, challenges encountered and the current suitability and future potential of the different setups for long-term in-situ measurement under field conditions are discussed.

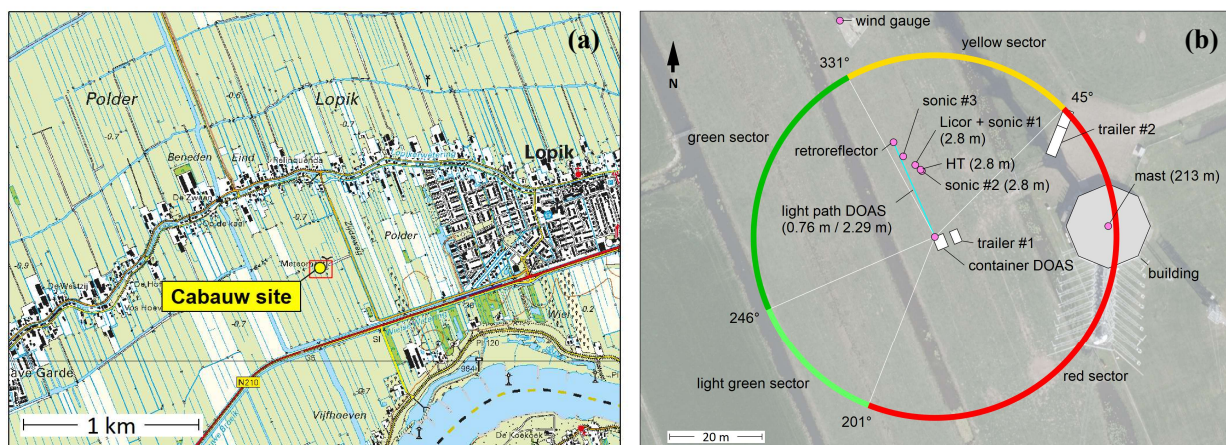
## 2 Campaign setup and site

### 2.1 Site description

NH<sub>3</sub> measurements were performed at the Cabauw site for atmospheric research (51.97034° N, 4.92559° E, elevation -0.7 m a.s.l.). The site is operated by Royal Netherlands Meteorological Institute (KNMI) and has been an atmospheric research station for over half a century (Bosveld et al., 2020). It hosts an extensive suite of meteorological and atmospheric instrumentation, some on the 213 m high mast on the facility. It is also one of the stations of the Dutch National Air Quality Monitoring Network and since 2019 part of the Ruisdael observatory (<https://ruisdael-observatory.nl/the-rita-2021-campaign/>, last access date: 20 Apr 2022). The site is 15 and 25 km away from the urban areas of Utrecht and Rotterdam, respectively (Figure S1). The area is completely flat (slopes less than 3%), with ribbon-shaped villages built along minor watercourses. Land use in the general area is predominantly agricultural, with most plots intensively managed grassland with an average vegetation height of 0.1 m used to graze cattle or sheep, or for silage. The soil consists of 35-50% river clay in the top 0.6 m, overlying a thick layer of peat (Bosveld, 2020). The soil of the top layer (0-0.15 m) has a bulk density of 1.14 g cm<sup>-3</sup> (Jager et al., 1976). The measurement site is drained by narrow (1-3 m) parallel ditches, which are on average 40 m apart.

To illustrate the distribution of the different land cover classes within the footprint of the instruments, an unsupervised land use classification is provided in Figure S2 of the supplementary materials. Moreover, Figure S3 illustrates the differences in management of individual paddocks in the flux footprint through time. During the campaign, sheep were grazing the plots of land immediately surrounding the measurement site. To prevent sheep from blocking the miniDOAS optical paths or from damaging instrument cables, the measurement area was secured with a low profile electric fence. These sheep often grazed

125 within 100 m north to northeast of the instruments with about 50 animals per hectare. Furthermore, the plots surrounding the research site were occasionally manured by local farmers, which was allowed up until September 15.



130 **Figure 1.** The area surrounding the Cabauw measurement site (a). Cabauw is in a flat area at -1m, being in the delta of the river Lek shown in the south east. The line with housing going east-west, running north of the tower has a series of farms. Map from [www.pdok.nl/](http://www.pdok.nl/) (downloaded 07-02-2021). The locations of the instruments (b). The coloured circle denotes wind origin sectors which are used for filtering data (see text). The green and light-green sectors indicate wind directions with minimally obstructed flow. Wind from the yellow sector is somewhat obstructed. Wind from the red sector experiences severe obstruction due to the building at the foot of the tall mast, the trailers and the DOAS container. Background aerial photo from [opendata.beeldmateriaal.nl](http://opendata.beeldmateriaal.nl) (downloaded 22-02-2022). Data of sonic #3 is not used in the final analysis.

## 135 2.2 Instruments overview

For this campaign, the following instruments were set up in a field next to the 213 m mast at Cabauw. The two miniDOAS NH<sub>3</sub> instruments were placed above each other in a small container (see below for a detailed description of these instruments). The 22.1 m optical paths were directed at 336°, parallel to the ditches between the fields. The bottom path was at 0.76 m and the top path 2.29 m above the field. Anticipating prevailing winds from the south-west, the other instruments were positioned  
140 3 m east of the miniDOAS optical paths (Figure 1), to minimise distortion of the incoming airflow. The instruments each integrated spectra during 4 minutes and provided simultaneous path-averaged concentration values at 4-minute intervals. These concentrations were then averaged to 30-minute values. The HT8700E open-path NH<sub>3</sub> analyser (see below for a detailed description of this instrument; hereafter referred to as ‘HT’), was mounted on a steel mast with the centre of its optical path at 2.80 m above the ground. On a second steel mast, 1.5 m from the first, a sonic anemometer (sonic #1; model Gill  
145 WindMasterPro™, Gill Instruments, Lymington, UK) was mounted. This sonic measured the 3D wind components at 32 Hz 2.8 m above the ground. The 10 Hz open-path H<sub>2</sub>O and CO<sub>2</sub> analyser (LI-7500DS, LI-COR Biosciences, Lincoln, USA) was placed at 2.83 m above the ground next to sonic #1.

From September 30 onwards, to evaluate the impact or sensor separation between the HT and the sonic #1 on the calculated  
150 NH<sub>3</sub> fluxes, a second sonic anemometer (sonic #2, model Gill WindMaster™, Gill Instruments, Lymington, UK) measuring at 32 Hz was installed 40 cm from the HT analyser.

In Figure 1 we show different coloured wind sectors. The selection is based on objects on the site that influenced the wind field and thus the flux intercomparison. The four wind sectors (Figure 1) were:

- 155 a) The green sector (246°–331°): minimal disruption. Only the drainage ditches are expected to influence the wind field.  
b) The light green sector (201°–246°): minimal disruption. We expected the DOAS container to have some influence.  
c) The yellow sector (331°–45°): some disruption. The masts with HT and the sonics disturbed the wind field at the DOAS paths. At times, the sheep farmer positioned a small trailer there on the field to the north of the 213 m mast, and sheep were grazing there. This would have affected all instruments.

- 160 d) The red sector ( $45^{\circ}$ – $201^{\circ}$ ): severe disruption. The 213 m mast, the building at the foot of this mast, the trailers and the DOAS container all affected all instruments.



165 **Figure 2.** The instruments, seen from the miniDOAS container looking north. From left to right: 10 m wind vane mast, mast with the two retroreflectors of the miniDOAS instruments, mast with sonic #3, mast with sonic #1 and LI-7500DS; mast with HT8700E and its cooling unit. Sonic#2 was placed later at 40 cm on the southeast side of HT8700E on the same mast (not shown in the photo). The 213 m mast is off to the right (east).

### 2.3 Weather conditions

Historically, winds from the southwest tend to be most common in September. During the campaign, the weather was slightly warmer and substantially drier than normal for this time of year (Homan, 2021) (Figure S4). However, there were no extremely hot or cold spells. No significant precipitation occurred during the measurement period, except for a few short shower events late September. The wind direction during the campaign was variable and therefore different from the expected predominant wind direction.

## 3 Methods

### 3.1 Aerodynamic gradient method (AGM) $\text{NH}_3$ fluxes

#### 175 3.1.1 MiniDOAS instruments

DOAS, short for differential optical absorption spectroscopy, is an optical technique to measure trace gas concentrations over an open path in the atmosphere (e.g. Platt and Stutz, 2008). For this experiment, two identical RIVM miniDOAS 2.2D instruments were used. These are active DOAS systems, i.e., equipped with their own light source rather than using sunlight. The light is sent to a retroreflector over an open path of 22.1 meters and received back (Figure 3). Path-averaged  $\text{NH}_3$  concentrations are retrieved from spectra taken in the 200–230 nm wavelength range.

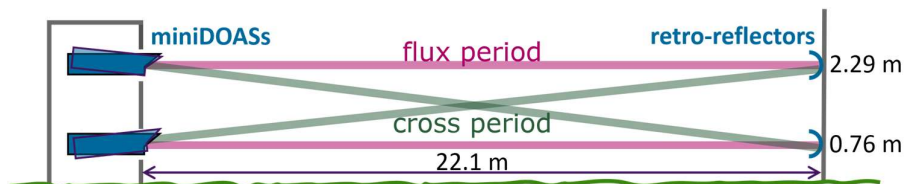


Figure 3. MiniDOAS setup in the field, using two instruments at different heights above the ground. The  $\text{NH}_3$  flux is determined from the observed concentration difference between top and bottom paths and the turbulence measurements of sonic #1 (flux period, shown in purple). Shown in green are the two instruments in cross-position (cross period). These zero-difference measurements are used for the precise intercalibration needed for flux measurements (see text).

185

The 2.2D instruments are a modified and further developed version of the miniDOAS 1.x described earlier (Berkhout et al., 2017; Volten et al., 2012b). MiniDOAS 1.x instruments have been operating in the Dutch national air quality monitoring network since 2016 at six locations. The uptime of these instruments in 2021 was above 95% of the hourly values.

190

Improvements in the 2.2D version include the use of a more sensitive charge-coupled device detector and several optical components with higher reflectivity and/or transmission in the wavelength range used, leading to about a factor of 5 increase in optical throughput. The optical layout was simplified and an optical scanner was added, making the system less sensitive to small alignment changes. These modifications resulted in a substantial increase in precision and stability of the measurements, as was needed for the monitoring of dry  $\text{NH}_3$  fluxes with the AGM method. We aim to describe the miniDOAS 2.x in more detail in a forthcoming publication, in combination with the implementation of this version in the Dutch national air quality monitoring network LML.

195

### 3.1.2 MiniDOAS calibration and intercalibration

As the AGM method depends on the ability to measure small concentration differences between two heights, great care must be taken to calibrate the two miniDOAS instruments properly, first individually and then as a pair, and to maintain this calibration over the flux measurement period. This process is described below.

200

#### 3.1.2.1 Initial individual lab calibration

Each instrument was calibrated according to the procedures used in the LML-network. This included the acquisition of a 'reference spectrum' with known, preferably zero, concentrations of  $\text{NH}_3$ ,  $\text{SO}_2$  and  $\text{NO}$ . For this, the zero-tunnel calibration facility at RIVM was used. This spectrum served as a common reference for all measurements. We also acquired 'calibration spectra' of the three gases mentioned, using a flow cell in the light path in combination with the zero-tunnel facility. These spectra contain the spectral fingerprint and cross-section of these gases, used in the analysis. For this step, calibration gases of these components with a supplier-indicated accuracy of 2% were used.

205

Afterwards, the accuracy of the  $\text{NH}_3$  calibration was tested by providing two  $\text{NH}_3$  mixtures in  $\text{N}_2$  from certified reference cylinders, representing a low and a high concentration of about  $35 \mu\text{g m}^{-3}$  and  $350 \mu\text{g m}^{-3}$  in the atmosphere, respectively (Certified Reference Materials, produced by the Dutch metrological institute VSL). These reference cylinders have a certified accuracy of 3% and 2% respectively. The instrument calibration was considered valid if the measurement result was within 3% of the certified reference.

210

#### 3.1.2.2 Additional intercalibration for deposition

While suited for concentration monitoring, the calibration approach above is not precise enough for AGM, where concentration differences of  $0.1 \mu\text{g m}^{-3}$  or better need to be determined, i.e., well below the 1% level. For this, an additional calibration of the two miniDOAS instruments is needed, as a pair. This was done after installation in the field.

215

The instruments were manually set to a different alignment position, as indicated in Figure 3, the so-called cross-position. As both instruments now sample on average the same height region, results should be identical for all flow situations where the  $\text{NH}_3$  gradient is homogeneous over the horizontal path. In this cross-setting, the instruments were set to run for several days,

220

until a sufficient amount of variation in outside air concentrations were encountered. Typically, the intercalibration lasts at least 3 days under suitable conditions.

225 First, new simultaneous reference spectra for both instruments were obtained from the dataset obtained during the intercalibration, to replace the reference spectra obtained in the zero-tunnel. The obtained absolute concentration values from these spectra will be less accurate, i.e., they may have a small but fixed offset to the lab. They will however be more precise which is essential for gradient measurements. Next, the spectra obtained in the cross period were processed with these new reference spectra

230 When comparing the results from both instruments in a scatter plot, the minor additional corrections to the offset and span can be obtained that are needed to make the instruments match perfectly, with offset 0 and slope 1.

In the Results section (Sect. 4.1), it will be illustrated that after these steps the pair was capable of measuring NH<sub>3</sub> differences within our target precision of 0.1 µg m<sup>-3</sup>. The new field reference spectra and the small additional corrections obtained in the cross-position are kept and also applied in the analysis of the flux measurements obtained in the parallel position.

### 235 3.1.3 Flux calculation

The 30-minute concentration measurements obtained at the two measurement heights were combined with 30-minute averaged transfer velocities to obtain the AGM NH<sub>3</sub> flux  $F_{AGM}$ , (e.g. Trebs et al., 2021):

$$F_{AGM} = -\frac{ku_*}{\ln\left(\frac{z_2}{z_1}\right) - \Psi_H\left(\frac{z_2}{L}\right) + \Psi_H\left(\frac{z_1}{L}\right)} \times [c_{NH_3}(z_2) - c_{NH_3}(z_1)] \quad \text{Eq. 1}$$

Where  $u_*$  is the friction velocity;  $k$  is Von Kármán constant (0.4),  $c_{NH_3}(z_n)$  is the NH<sub>3</sub> concentration at height  $z_n$ ;  $z_1$  and  $z_2$  are the heights of the bottom and top miniDOAS paths above the displacement height  $d$  (assumed 2/3 of the canopy height),  
240 respectively.  $\Psi_H\left(\frac{z}{L}\right)$  is the integrated stability function for heat, which is assumed to be the same for NH<sub>3</sub>.  $L$  is the Monin-Obukhov length. For unstable conditions ( $L < 0$ ), we used the functions of Dyer (1974) and Paulson (1970). For stable conditions ( $L > 0$ ), we used the function of Beljaars and Holtslag (1991). Micrometeorological parameters  $u_*$  and  $L$  were calculated using EddyPro software version 7.0.6 (LI-COR Biosciences, Lincoln, USA) using data collected by sonic #1. AGM fluxes were calculated using custom software written in R. We follow the sign convention where positive fluxes indicate  
245 emissions and negative fluxes deposition.

## 3.2 Eddy covariance (EC) NH<sub>3</sub> fluxes

### 3.2.1 HT8700E instrument

The open-path QCL-based NH<sub>3</sub> analyser (Healthy Photon Lt. Co., Ningbo, China, Model HT8700E; hereafter HT) was used to measure NH<sub>3</sub> concentrations at 10 Hz using the wavelength modulation spectroscopy technique. Technical details of the  
250 analyser have been described in Wang et al. (2021). The QCL sends a beam at 9.06 µm into an open-air Herriott cell which has two concave mirrors of high purity molybdenum with a coating that should withstand frequent cleaning with organic detergents. The temperature of the QCL and detectors are stabilized by Peltier thermo-electrical coolers (TEC). The analyser is coupled to a compact external water and ethylene glycol chiller (Wang et al., 2021).

The HT8700 performance in laboratory and field experiments has been presented by Wang et al. (2021, 2022). The uncertainty  
255 of the NH<sub>3</sub> concentration measurements was estimated to be ±15% by comparing two commercially available high-sensitivity NH<sub>3</sub> analysers G2103 (Picarro Inc., Sunnyvale, USA) and EAA-911 (Los Gatos Research (LGR), San Jose, USA) in the lab (Wang et al., 2021). In the follow-up study (Wang et al., 2022), a slightly higher noise ratio ( $0.41 \pm 0.06$  ppbv) and flux

detection limit ( $9.6 \pm 1.5 \mu\text{g N m}^{-2} \text{h}^{-1}$ , equivalent to  $3.2 \pm 0.5 \text{ ng NH}_3 \text{ m}^{-2} \text{s}^{-1}$ ) were found after one-month long monitoring at a wheat field in Northern China.

260 Raindrops, dust, and other contaminants on the mirrors (particularly the bottom one), cause light scattering which is shown in the optical signal strength (OSS) of the HT (Wang et al., 2021). In contrast to Wang et al. (2021, 2022) in this experiment we used an upgraded HT version being equipped with an automated mirror cleaning system (the SPIDER<sup>®</sup>) that can be activated remotely, which significantly reduced the manual cleaning burden. During this campaign whenever the OSS value dropped below 40% the lower mirror was cleaned using the SPIDER<sup>®</sup> for 1 to 2 minutes at a time. In addition, both mirrors were  
265 manually cleaned 1-2 times per week using lens tissue drenched in methanol if automatic cleaning was not sufficient. However, the OSS values gradually decreased over the experimental period especially after multiple rain events before the end of the campaign (Figure S5).

### 3.2.2 Flux calculation

The EC NH<sub>3</sub> fluxes and other micrometeorological parameters were calculated using EddyPro software (version 7.0.6, LI-  
270 COR Biosciences, Lincoln, USA) at 30-minute intervals using the 10 Hz ‘raw’ data. The general flux calculation procedure followed the standard FluxNet methodology (Mcdermitt et al., 2011) and some basic settings are following Wang et al. (2021). For detailed settings and parameters of this study see Table S1. In addition to the analysis in EddyPro, additional spectral analyses were further tested to study the impact of high-frequency spectral damping and sensor separation on the flux results.

#### 275 3.2.2.1 High frequency spectral losses correction

The eddy flux method evaluates the vertical transport of gas, heat or momentum caused by a composition of turbulent eddies that cover the spectrum from cm to km scale or, in the time domain, from 10 Hz to 30 min scale. Measured EC fluxes correlate the vertical wind and the concentration variation, the covariance which can be visualised in a cospectrum showing the contribution of the large and small turbulent motions. The raw measurement data need corrections for turbulence-spectral  
280 losses both in the low (> minutes) and high (> 1 Hz) -frequency range. For the open-path system, the former is caused by the finite averaging time, as the measurement system will not “see” large scale eddies that take longer than the 30-minute evaluation interval. The concentration changes that occur with a high frequency (linked to small eddies) are dampened due to the sensing volume of the instrument (which is 50 cm high and will not show eddies that are 10 or 5 cm in diameter) and due to the spatial separation between sonic anemometer and gas analyser (Moore, 1986).

285 Using the EddyPro software, low-frequency flux losses were corrected according to Moncrieff et al. (2004). For estimating high-frequency flux losses, the theoretical method from EddyPro (hereafter referred to as TEO; Moncrieff et al., 1997) was applied first. Two remarks have been made on this procedure. First, a difference can occur between the measured cospectra and the theoretical frequency distribution of Kaimal cospectra (Kaimal et al., 1972; Moncrieff et al., 1997). Second, in EddyPro’s implementation of Moncrieff et al. (1997) the correction for sensor separation is independent of the wind direction,  
290 which holds as long as the distance between the sonic anemometer and gas analyser is relatively small (Moore, 1986). Moore (1986) already indicated that in doing so the flux correction would probably be overestimated. Therefore, to better understand the real field condition and equipment separation results in EC flux, an empirical approach using measured gas flux cospectra and sensible heat cospectra as reference was applied similar to Wintjen et al. (2020, hereafter referred to as ICO after ‘in situ cospectral method’)). For detailed ICO method data quality control, see Sect. 1.1 in the supporting materials.

295

#### 3.2.2.2 Modified WPL correction

Open-path trace gas concentrations are affected by density variations in the up- and down going air movements. The Webb-Pearman & Leuning (WPL) correction accounts for that (Webb et al., 1980). Two WPL methods were used. First, the classic WPL method was used to correct H<sub>2</sub>O measurements from LI-7500DS. Part from that, the NH<sub>3</sub> flux is also affected by



300 spectroscopic effects (Burba et al., 2019). The spectroscopic part is instrument dependent and deals with the effect of changing H<sub>2</sub>O concentrations and their impact on the absorption line used for NH<sub>3</sub>. Hence, the modified WPL method was applied to correct the HT-measured NH<sub>3</sub> flux following Wang et al. (2021):

$$F_{EC} = A \left[ \overline{w' \rho'_A} + B \mu \frac{\overline{\rho_A}}{\overline{\rho_d}} \overline{w' \rho'_v} + C \left( 1 + \mu \frac{\overline{\rho_v}}{\overline{\rho_d}} \right) \frac{\overline{\rho_A}}{\overline{T_a}} \overline{w' T'_a} \right] \quad \text{Eq. 2}$$

305 where  $\rho_A$  is the NH<sub>3</sub> density corrected for temperature (see Sect. 4.1.2),  $\rho_d$  is the dry air density,  $\rho_v$  is the water vapor density,  $\mu$  is the molar mass ratio of dry air to water vapour,  $\overline{w' \rho'_v}$  is the water vapour flux measured by the LI-7500DS,  $T_a$  is the air temperature and  $\overline{w' T'_a}$  is the sensible heat flux from the sonic anemometer.  $A$ ,  $B$ , and  $C$  are dimensionless parameters accounting for the spectroscopic effects from (Wang et al., 2021), which vary with ambient temperature, pressure and water vapour content.

### 310 3.3 Quality control and filtering

Firstly, observations from the HT were filtered out before the EC flux analysis if the optical signal strength (OSS) of the NH<sub>3</sub> analyser was below 40% (Figure S5). Secondly, after EC analysis in EddyPro was completed, EC fluxes were removed if a quality flag of 2 was assigned according to the stationarity and integral turbulence tests proposed by Mauder and Foken (2006). Thirdly, both fluxes with  $u_*$  values smaller than 0.1 m s<sup>-1</sup> were discarded, to filter out observations during low-turbulent mixing  
 315 conditions. Fourthly, a moving window outlier filter was applied to the remaining fluxes, removing points if two times the standard deviation of the adjacent six flux values was exceeded (Wang et al., 2021; Wang et al., 2022). Finally, the data was grouped into 4 different wind sectors (green, light green, yellow and red) as described in Figure 1. Only observations from the green and light green sectors were used for the intercomparison of the fluxes. An overview of the applied filters and the percentage of accepted fluxes per filter step are shown in Table S2 in the supplementary materials.

### 320 3.4 Uncertainty analysis

A description of the random error analysis of the half-hourly AGM and EC fluxes is given in Sect. 1.2 of the supporting materials.

### 3.5 Footprint analysis

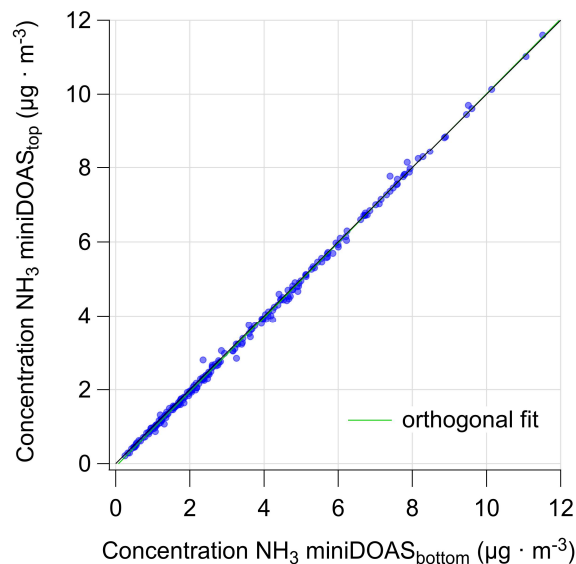
The footprint of the EC fluxes showing the contributing area of measured fluxes was analysed following the method from  
 325 Kljun et al. (2015). Inputs for this method include the EC measurement height ( $z = 2.80$  m), roughness length (assumed to be 0.15 times canopy height), friction velocity ( $u_*$ ), the Obukhov length, the standard deviation of the lateral wind ( $v$ ) component, wind direction, mean wind speed, and the boundary layer height. Apart from the boundary layer height, other parameters were measured by the EC system. The hourly boundary layer height data was obtained from Climate Data Store (CDS) source (ERA5 hourly data: <https://cds.climate.copernicus.eu/cdsapp#!/dataset/reanalysis-era5-single-levels>, last access date: 1 Feb  
 330 2022) and the hourly values were linearly interpolated to half-hourly values for the footprint calculation. The flux footprint prediction (FFP) method (<http://footprint.kljun.net>, last access date: 1 Feb 2022) was used for coding and plotting. Here, footprints were only determined for EC NH<sub>3</sub> flux after quality filtering (see Sect. 3.3). No separate footprint analysis was done for the AGM fluxes.

## 4 Campaign results

### 335 4.1 NH<sub>3</sub> concentrations

#### 4.1.1 MiniDOAS intercalibration

The lab calibration procedure of both individual miniDOAS instruments is described in the instrument section (Sect. 3.1.2). Here, the result of the intercalibration in the field is shown, which aims to increase the precision of the concentration difference measurement further. Intercalibration measurements were taken in three periods: at the beginning and end of the campaign and  
340 once during the campaign. In total, 35% of the 7-week uptime was spent on intercalibrations. The data was filtered for well-mixed situations ( $u_* > 0.1 \text{ ms}^{-1}$ ) and obstacle-free wind directions (green and light green) in order to obtain homogenous concentration gradients along the path. Figure 5 shows a scatter plot of the obtained concentration measurements by both instruments matching these requirements.



345 **Figure 4. Scatter plot of data obtained by the two miniDOAS instruments during all three cross-periods. Data was filtered to include only obstacle-free wind directions and turbulent conditions ( $u_* > 0.1 \text{ m s}^{-1}$ ). Using an orthogonal fit, an offset of  $0.07 \pm 0.01 \mu\text{g m}^{-3}$  and a slope of  $1.009 \pm 0.002$  (the green line) was found.**

The offset and slope correction were applied to the concentrations of miniDOAS<sub>top</sub> over the full campaign. The standard deviation of the residuals was used as an estimate of the remaining random uncertainty in the concentration difference  
350  $c_{\text{NH}_3}(z_2) - c_{\text{NH}_3}(z_1)$  after correction. This random error was determined to be  $0.088 \mu\text{g m}^{-3}$ .

The results of the intercalibration periods are discussed in section S1.3 of the supporting materials. The conclusion is that, over the full campaign period, the zero-level of the difference measurement has been stable, and the individual difference measurements showed a typical spread of  $0.1 \mu\text{g m}^{-3}$  or less.

#### 4.1.2 HT concentration corrections

355 The HT NH<sub>3</sub> concentration measurement contained a considerable amount of gaps in the data (21% during the 5-week uptime). These gaps largely occurred during rain and mirror cleaning afterwards. At the start of the campaign, the HT instrument had an offset of about  $-7 \mu\text{g m}^{-3}$  (data not shown). After the campaign, the analyser was recalibrated in the lab and the ‘zero’ was found to be  $-6.3 \pm 0.3 \mu\text{g m}^{-3}$  when flushing pure nitrogen gas for 6 hours through the calibration cell while the temperature was kept constant at  $17 \text{ }^\circ\text{C}$ . Before temperature correction, raw HT and miniDOAS<sub>top</sub>’s average difference was  $-5.3 \mu\text{g m}^{-3}$  (range  
360  $-15$  to  $6 \mu\text{g m}^{-3}$ ,  $n = 1180$ ) during the overlapping period of the campaign. The raw half-hourly HT NH<sub>3</sub> concentrations showed inconsistent differences compared to the miniDOAS concentration levels, which varied with air temperature. After applying a

third-order polynomial fit of the HT-miniDOAS concentration difference versus temperature, the corrected concentrations for HT were finally obtained (Figure S7). Temperature mainly impacted on the offset of its concentration and it seemed to have a negligible influence on the span of the HT's concentration (slope  $\approx 0.97$ , Figure 7).

### 365 4.1.3 Comparison miniDOAS and HT concentrations

After application of the temperature correction on the  $\text{NH}_3$  concentrations of the HT, the concentration of the two instruments were very similar ( $R^2 = 0.97$ , Figure 7). Furthermore, the time series of the corrected  $\text{NH}_3$  concentrations from both instruments captured the same temporal pattern and peak events. The highest concentrations are observed during night-time when the boundary layer height is small and vertical mixing is limited. During daytime the concentrations decrease due to the rise of the  
 370 boundary layer and the increased vertical turbulent transport (Figure 8).

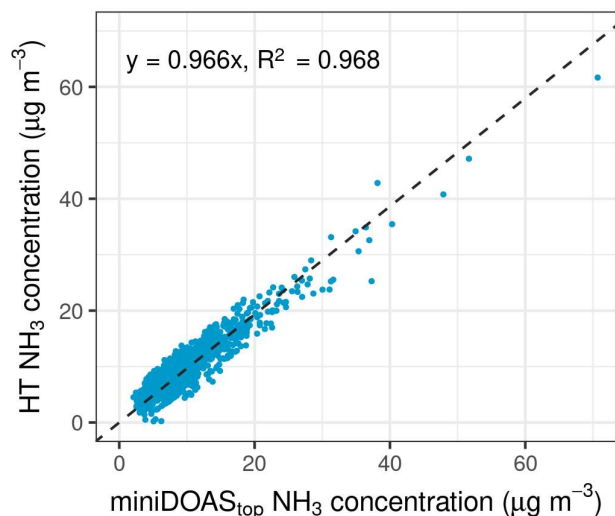
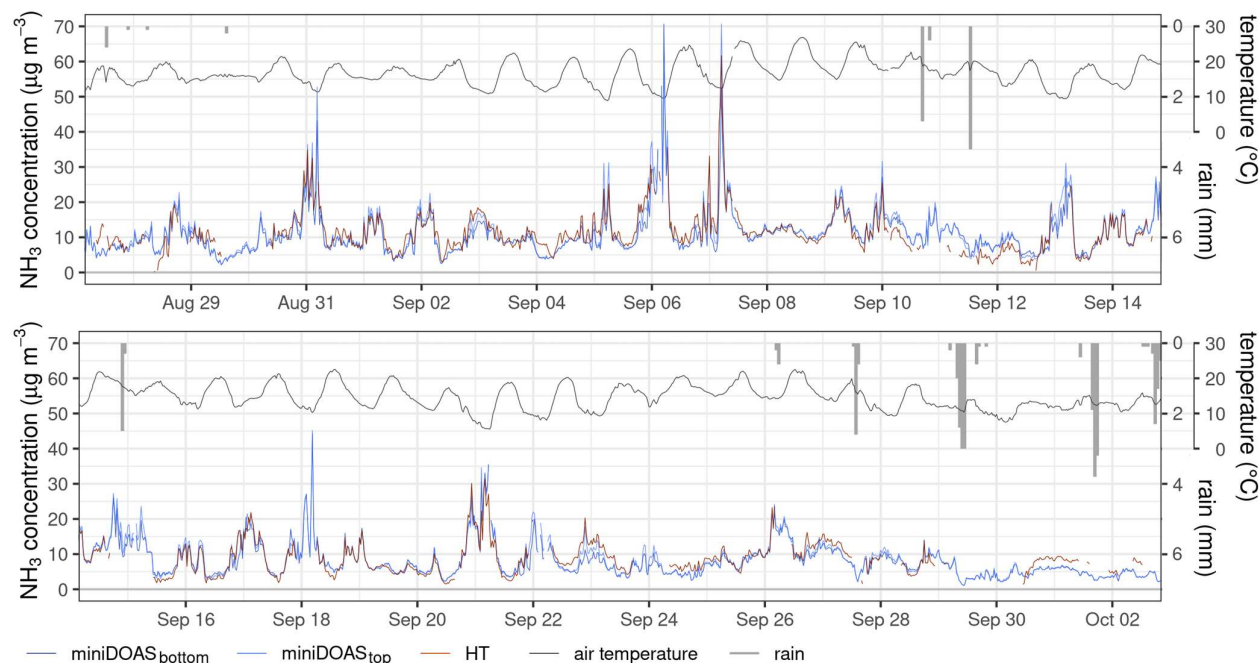


**Figure 5** Scatter plot of the  $\text{NH}_3$  concentrations from the  $\text{miniDOAS}_{\text{top}}$  and the temperature corrected HT instrument during parallel measurements (correlation line was forced through the origin).



375 **Figure 6.** Time series of the measured, unfiltered  $\text{NH}_3$  concentrations after temperature correction from the HT (red) and the  $\text{miniDOAS}$  instruments (dark blue for the bottom one; light blue for the top one) in  $\mu\text{g m}^{-3}$ , the hourly ambient temperature (black) in  $^{\circ}\text{C}$  and the amount of rainfall (grey bars) in mm.

## 4.2 Uptime, filtering and quality control

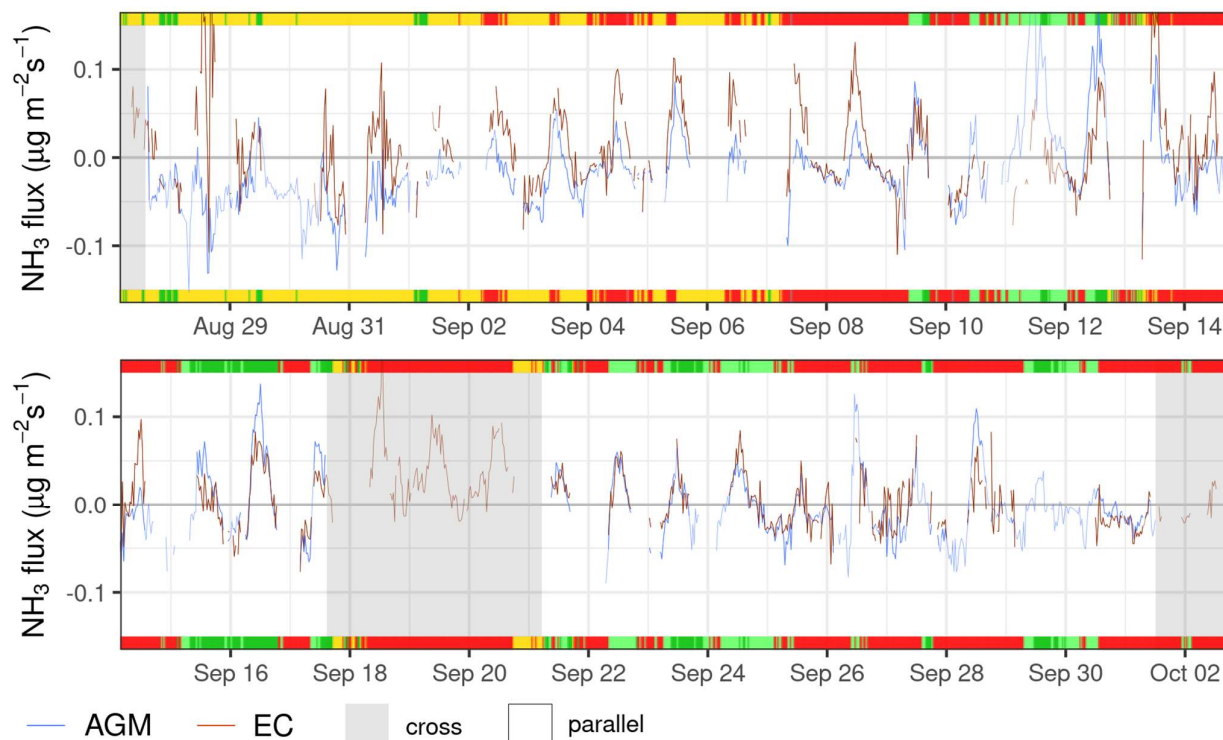
380 For the AGM method, the vertical  $\text{NH}_3$  concentration gradient measured by the miniDOAS instruments and the transfer  
velocity from the sonic #1 anemometer were used to determine the  $\text{NH}_3$  flux. Figure S8a in the supplementary materials shows  
the full time series of the  $\text{NH}_3$  flux derived using the miniDOAS setup. The miniDOAS setup had an uptime of nearly 100%  
over the full campaign (1142 hours). Except for the 35% intercalibration period, 80% of the remaining parallel measurements  
(597 hours) were left after filtering out low turbulent mixing conditions ( $u_* < 0.1 \text{ m s}^{-1}$ ) and outliers. For the EC  $\text{NH}_3$  flux  
385 measurements, Figure S8b shows the full time series. The uptime of the HT instrument was 79% during the 5-week field  
operational period (685 hours). After filtering for fluxes with poor quality flags,  $u_* < 0.1 \text{ m s}^{-1}$  and outliers, 59% of the valid  
observations remain (516 hours). Observations on the 11<sup>th</sup> of September were excluded due to large differences between the  
measured fluxes on that day, although they originated from green wind directions. We assume this was related to manuring at  
the adjacent field that might have disturbed the footprint homogeneity of the flux but we have no evidence to support that.  
390 After filtering, 848 overlapping half-hours were left for flux comparison between two instruments.

## 4.3 Comparison of the AGM and EC fluxes

Both  $\text{NH}_3$  fluxes are shown in Figure 9. Here, the EC fluxes corrected for flux damping in EddyPro are shown, which is  
considered as a reference method. After quality control filtering, the EC and AGM fluxes have a similar range and pattern.  
Within the green and light green sectors, the highest  $\text{NH}_3$  emission measured with the AGM setup was  $0.18 \mu\text{g m}^{-2} \text{ s}^{-1}$  and  
395 deposition was  $0.15 \mu\text{g m}^{-2} \text{ s}^{-1}$ . The highest observed  $\text{NH}_3$  emissions with the EC setup was  $0.16 \mu\text{g m}^{-2} \text{ s}^{-1}$  and deposition was  
 $0.10 \mu\text{g m}^{-2} \text{ s}^{-1}$ .

At the start of the measurement period, the AGM and EC fluxes were quite different. During the first days, the miniDOAS  
system presented  $\text{NH}_3$  deposition, while the HT showed  $\text{NH}_3$  emissions. In this period, the prevailing winds were from the  
400 north/northeast, categorised as yellow (see Figure 1), where sheep were occasionally located upwind of the instruments. This  
may have caused inhomogeneity of the source/sink pattern within the footprint area (see below), which would have violated  
the AGM/EC calculation assumptions. Furthermore, the  $\text{NH}_3$  concentrations during this episode were relatively high as  
manuring activities were still allowed until 15 September on the grasslands surrounding the measurement site. In the green  
and light-green wind directions, the  $\text{NH}_3$  fluxes from the two methods compared well after September 20<sup>th</sup> when little or no  
405 effect of manure application should be present.

Considering only high-quality measured fluxes during this period, the cumulative daily fluxes of the AGM and EC were in  
general similar, with typical differences in the order of  $\sim 10\%$  (Figure S9). When looking at the cumulative flux over the full  
period however, a larger difference is observed. This difference appears stepwise on a single day, September 24<sup>th</sup>. On this  
410 day, and only during a few hours around noon, we see a much larger flux observed by EC compared to AGM. Most likely, the  
discrepancy is caused by footprint issues in combination with very local emissions. Unfortunately, we lack the means to  
validate this assumption.

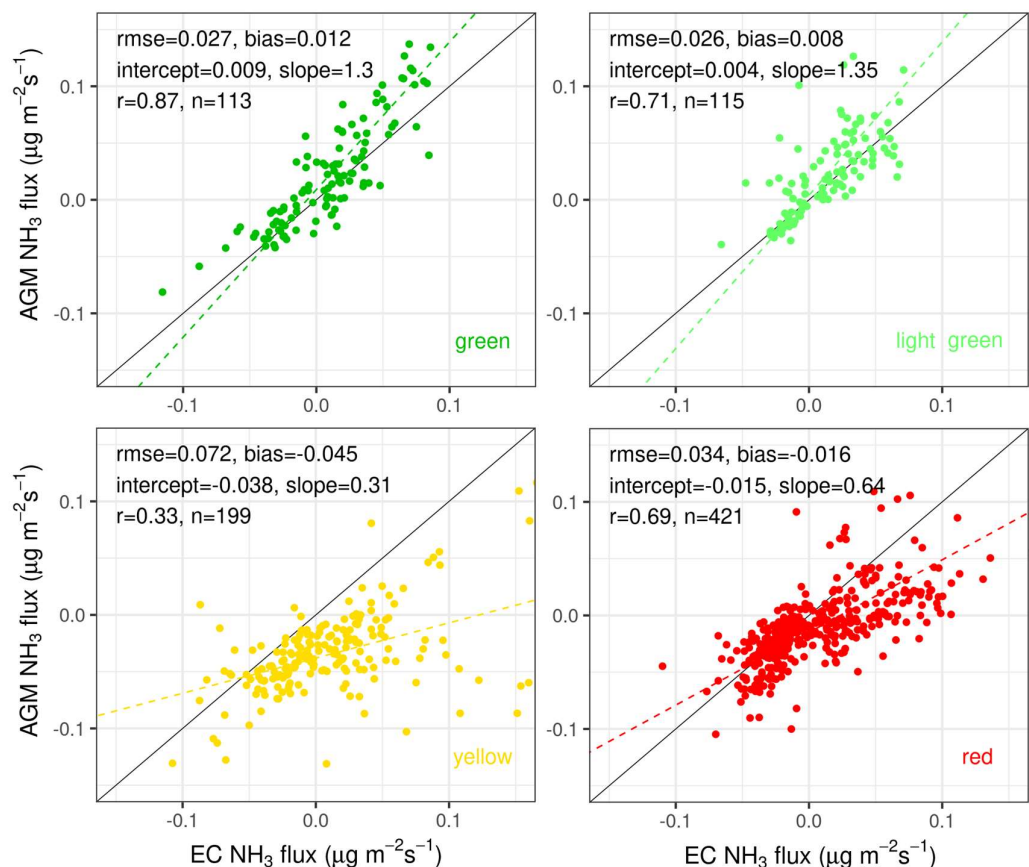


415 **Figure 7.** Timeseries of the  $\text{NH}_3$  fluxes of AGM with miniDOAS instruments (blue) and the EC method from the HT (red). Positive fluxes indicate emissions, negative fluxes deposition. The colours in the upper and lower borders indicate the prevailing wind directions from Figure 1. The intercalibration periods for the miniDOAS instruments are shown against a grey background. The thick lines indicate the  $\text{NH}_3$  fluxes that were left for intercomparison after all filters were applied.

Figure 10 shows the comparison of the EC (EddyPro calculated) and AGM  $\text{NH}_3$  fluxes per categorized wind direction. There is a strong correlation ( $r = 0.87$ ) between the EC and AGM  $\text{NH}_3$  fluxes at times where the airflow was unobstructed, i.e.,

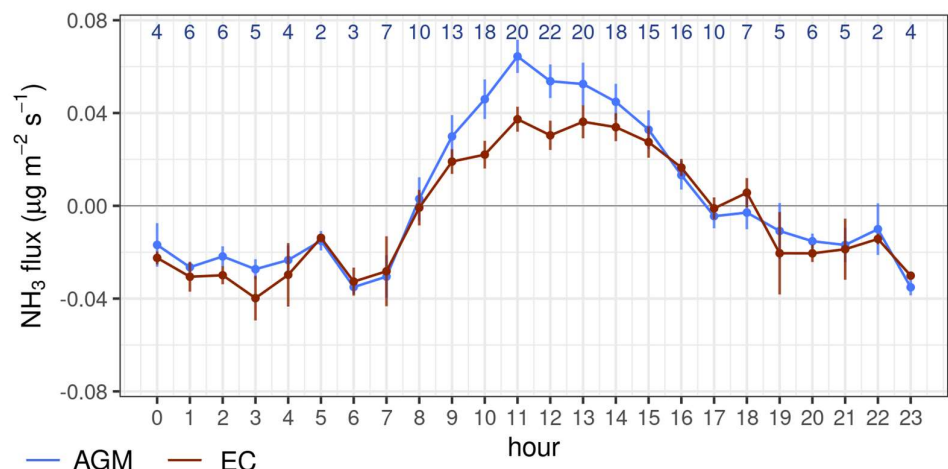
420 when the wind came from the directions categorized as green. In this category, the differences between the EC and AGM  $\text{NH}_3$  fluxes were relatively small ( $\text{RMSE} = 0.027 \mu\text{g m}^{-2} \text{s}^{-1}$ ,  $\text{bias} = 0.012 \mu\text{g m}^{-2} \text{s}^{-1}$ ), too. There is a moderate correlation between the EC and AGM  $\text{NH}_3$  fluxes in the light green ( $r = 0.71$ ) and the red categories ( $r = 0.69$ ). In both the green and light-green categories, the AGM based fluxes were approximately 30% above the EC based levels (slope = 1.3 (green) and slope = 1.35 (light green)). In the red category, the airflow was partially obstructed by large objects. In this category, the EC fluxes were

425 generally larger than the AGM fluxes (slope = 0.64), but relatively small differences ( $\text{RMSE} = 0.034 \mu\text{g m}^{-2} \text{s}^{-1}$ ,  $\text{bias} = -0.016 \mu\text{g m}^{-2} \text{s}^{-1}$ ) between the EC and AGM  $\text{NH}_3$  fluxes were found still. The poorest agreement ( $r = 0.33$ ,  $\text{RMSE} = 0.072 \mu\text{g m}^{-2} \text{s}^{-1}$ ,  $\text{bias} = -0.045 \mu\text{g m}^{-2} \text{s}^{-1}$ ) between the two methods is found for the yellow wind direction category. In this category, the HT often observed  $\text{NH}_3$  emissions while the miniDOAS setup observed deposition of  $\text{NH}_3$ .



430

**Figure 8 Comparison of the AGM NH<sub>3</sub> fluxes from the miniDOAS instruments and the EC NH<sub>3</sub> fluxes from the HT per categorized wind direction (see Figure 1).**



435

**Figure 9. Mean diurnal cycle of the EC and AGM NH<sub>3</sub> fluxes. Positive flux is emission, negative flux is deposition. The error bars indicate the standard error of the hourly means ( $\sigma/\sqrt{n}$ ). The number of hours averaged are listed in blue text at the top. Here, filtered NH<sub>3</sub> fluxes from only the green and light green wind directions where both systems have a valid flux observation were used. Data from the 11<sup>th</sup> of September is excluded, too, due to a potential emission event causing footprint heterogeneity.**

The two methods showed a similar diurnal pattern using NH<sub>3</sub> fluxes from the green and light green wind directions (Figure 11). NH<sub>3</sub> was generally emitted during the day and deposited during the night. Between 10:00 and 14:00, the AGM fluxes were a factor ~1.7 higher than the EC fluxes. Figure S10 in the supplementary materials shows the diurnal pattern using only data after September 15. The mid-day differences between the two are smaller, but still exist, even though manure spreading was not allowed anymore.

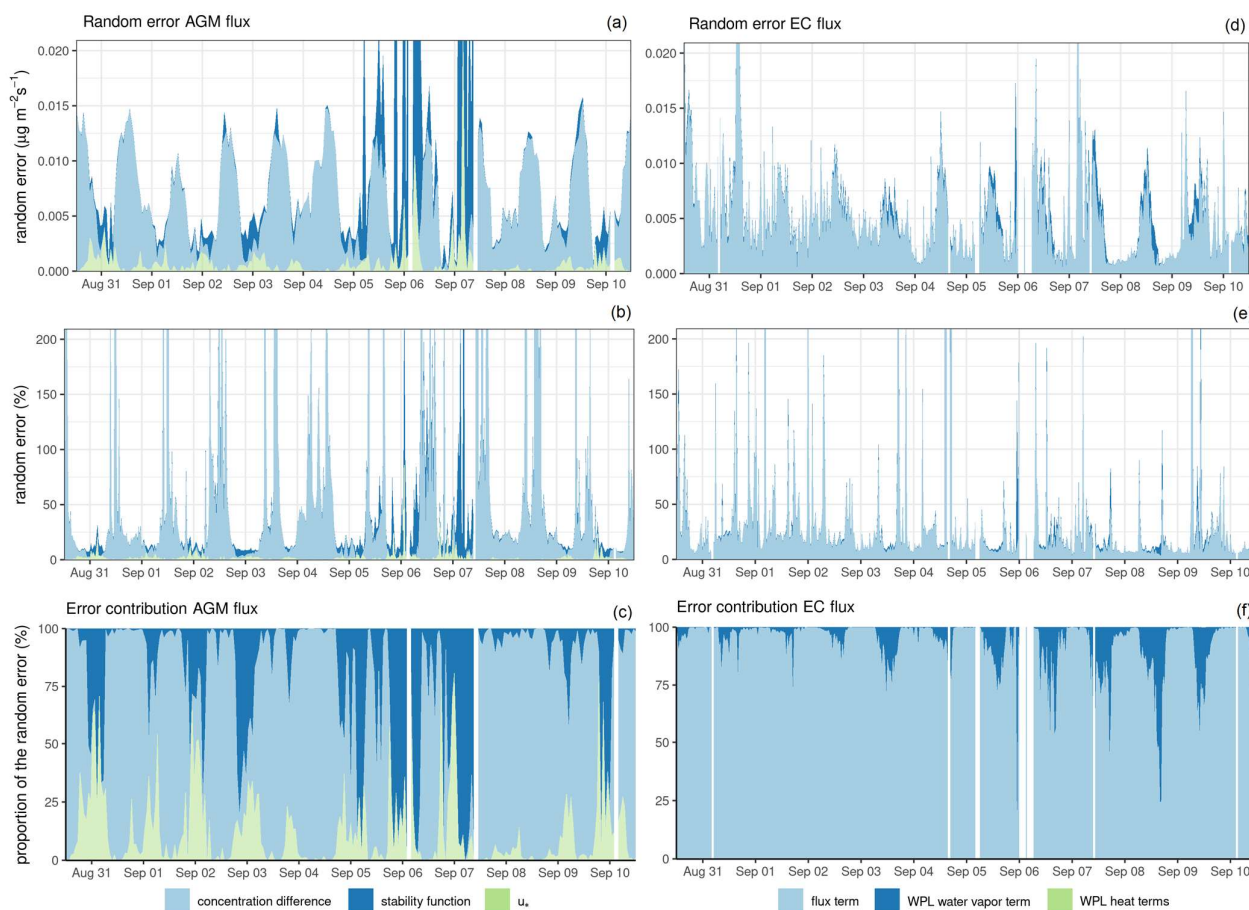
440

#### 4.4 Uncertainty analysis

Figure 12 shows the random errors of the AGM and EC NH<sub>3</sub> fluxes and the contribution of different components to the error. The random errors of the two showed a similar range of values. On average, EC NH<sub>3</sub> fluxes had a slightly lower error. The mean random error (1σ) of the AGM NH<sub>3</sub> flux was 15.0 ng m<sup>-2</sup> s<sup>-1</sup> (median 7.4 ng m<sup>-2</sup> s<sup>-1</sup>), while the mean random error of the EC NH<sub>3</sub> fluxes amounted to 5.5 ng m<sup>-2</sup> s<sup>-1</sup> (median 4.1 ng m<sup>-2</sup> s<sup>-1</sup>). The mean and median relative random errors were 89% and 24% for the AGM flux versus 61% and 15% for the EC flux.

The random errors of the AGM fluxes showed a clear diurnal pattern. During the daytime, the random errors were relatively large and peaked around noon, because the observed gradient was the smallest at this time. As a result, the measurement error in the NH<sub>3</sub> concentration differences dominated. During the night, the random errors were relatively small; here, the errors in the  $u_*$  values had a relatively large contribution. As a consequence, especially deposition estimates were sensitive to the random error in  $u_*$ . The largest random errors in the NH<sub>3</sub> fluxes largely took place when the error in the stability correction takes over, i.e. when a substantial stability correction was applied to the measurement heights of the miniDOAS instruments. This occurred occasionally during night-time, usually around midnight. Compared to the random error of the AGM NH<sub>3</sub> fluxes, the diurnal cycle of the random error in the EC NH<sub>3</sub> fluxes was less apparent. The contributions of the heat terms in the WPL correction to the total random error were negligible. The contribution of the error in the WPL water vapour term can be quite substantial (max. ~75%) in incidental cases but is generally between zero and ~20% during daytime.

460



465 **Figure 10. The absolute and relative random errors and the corresponding error contributions (in % of the random error) of the AGM (a, b, c) and EC (d, e, f) NH<sub>3</sub> fluxes from August 31<sup>st</sup> to September 10<sup>th</sup>. For the EC fluxes, the light blue component (flux term) refers to F1 in Eq. 4, based on fluxes determined using EddyPro, taking into account the damping correction and term A from Eq. 4.**

#### 4.5 Footprint analysis

The footprint of the EC NH<sub>3</sub> fluxes was computed at sonic #1's height using the method from Kljun et al., (2015) and shown in Figure 13a for all wind directions and in Figure 13b for only the green and light-green sectors. Overall, 80% of the flux originated from an area within approximately 100 meters distance from the measurement devices. Furthermore, the influence of the 213 m mast seems visible and reduces the footprint to the southeast. Because the highest measurement point has the largest footprint, the footprint of the miniDOAS instruments, especially miniDOAS<sub>bottom</sub>, will be substantially smaller. The measured fluxes are assumed to be representative of the footprint area. The largest footprint area determines the outside perimeter of the area within which the landscape should be homogenous. If that is not the case it can be expected that the AGM and EC methods will end up with different results.

475

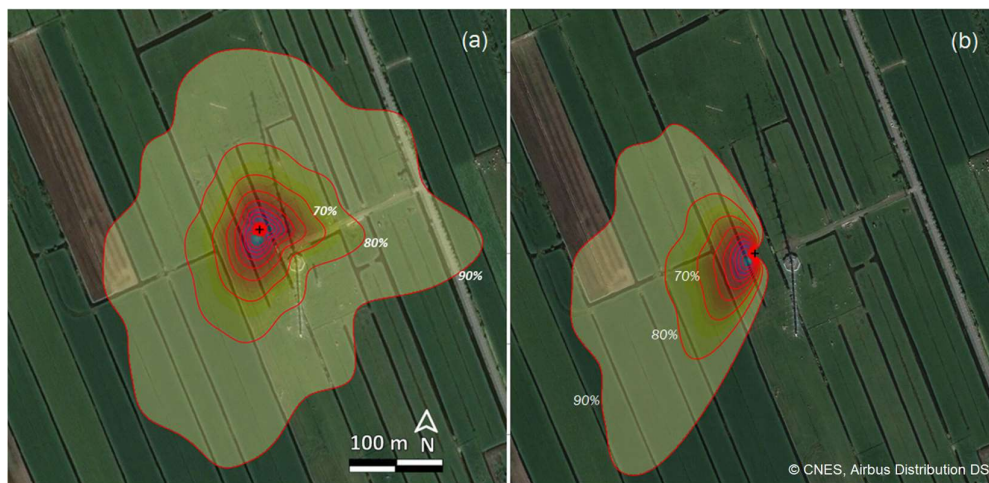


**Figure 11. EC footprint for (a) all wind sectors and (b) the green and light-green wind sectors Footprint climatology estimate of the EC measurements ( $z = 2.80$  m). The red curves are at 10% footprint contour lines. Background map data: Microsoft, CNES Distribution Airbus DS**

#### 480 4.6 Damping correction methods: TEO versus ICO for EC flux

To evaluate the effect of damping on the EC flux, both the theoretical method from EddyPro (TEO) and the empirical method (ICO) were used. In the results above we use the EddyPro theoretical approach (Table S1) since we consider that is the 'standard' evaluation method. The comparison showed that TEO corrections are larger than the ICO factors for CO<sub>2</sub>, H<sub>2</sub>O, and NH<sub>3</sub> (Figure S11). The sensible heat flux cospectrum indicates that the Kaimal cospectrum in TEO does not represent the turbulent characteristics of the site well enough (Figure S12). Application of the ICO method on the HT data however decreased correlations with the AGM results in the light green and green wind sectors (Figure S13). The ICO method seems to be conceptually better. However, ~50% of the dataset had to be corrected using daily median values, because the measurement-based ogives were noisy (caused by low flux conditions). We therefore decided for this relatively short campaign to still use the TEO method for the flux comparison with AGM method.

490

The damping is affected by both the sensor separation and the sensing volume. The HT and the combination of sonic #1 and LI-7500DS were 1.5 m apart during the entire campaign period. Using sonic #1 data, the HT instrument median flux damping of NH<sub>3</sub>, CO<sub>2</sub>, and H<sub>2</sub>O were 37%, 1%, and 1%, respectively according to ICO method. For sonic #2 which was installed at the end of the campaign for 2 days at 0.40 m distance to the HT and 1.35 m to the LI-7500DS ICO gave 16%, 32%, and 31% for NH<sub>3</sub>, CO<sub>2</sub>, H<sub>2</sub>O damping. So the separation between the HT and the sonic #1 caused ca. 20% extra damping for NH<sub>3</sub> flux. Separating the LI-7500DS and sonic #2 by the same distance caused 30% damping for the H<sub>2</sub>O and CO<sub>2</sub> flux. That could be explained because the HT has a 4 times longer vertical path length than the LI-7500DS sensor (0.50 m vs. 0.125 m) in which higher frequencies will be damped anyway.



500 The TEO method, applied for the two days with both sonics available, gave median damping factors 41%, 14% and 14% for NH<sub>3</sub>, CO<sub>2</sub>, and H<sub>2</sub>O using sonic #1 and 20%, 38%, and 37% using sonic #2. Both TEO and ICO methods produced the same damping difference between the two sonics for NH<sub>3</sub> flux (*ca.* 20%). As a consequence, the corrected NH<sub>3</sub> fluxes obtained with sonic #1 or sonic #2 were the same (see Figure S14) suggesting the damping correction provides reasonable flux estimates. When comparing the fluxes with sonic #1 during the entire campaign period, the TEO corrections for all gases were larger than the ICO ones (see Figure S11). For NH<sub>3</sub> flux losses were 39% versus 28%, respectively. Surprisingly, even without extra distance separation between LI-7500DS and sonic #1, TEO suggests 12% correction for the H<sub>2</sub>O and CO<sub>2</sub> flux while ICO only suggests 2-3% damping correction as average for the entire period.

## 5 Discussion

510 We had the unique opportunity to use two newly developed open-path instruments providing independent data for the NH<sub>3</sub> flux estimate. An overview of the main findings of the 5-week intercomparison campaign can be found in Table 1.

**Table 1. Overview of the main differences, strengths and weaknesses of the two instrument setups compared.**

	<b>miniDOAS using AGM</b>	<b>HT using EC</b>
<b>Field performance</b> <sup>*1</sup>	<ul style="list-style-type: none"> <li>• 100% uptime, 65% flux, 35% calibration (% calibration time can be reduced)</li> <li>• hands-off for 7 weeks during campaign</li> <li>• typical hardware maintenance: annual lamp and mirror replacement</li> <li>• ready for long-term monitoring deployment</li> </ul>	<ul style="list-style-type: none"> <li>• 79% uptime, no measurements during rain or dew</li> <li>• needs regular operator interventions (mirror cleaning)</li> <li>• substantial mirror degradation, replacement needed after 5 weeks<sup>*3</sup></li> <li>• not yet ready for long-term monitoring deployment</li> </ul>
<b>Flexibility in application</b> <sup>*2</sup>	<ul style="list-style-type: none"> <li>• needs housing and mains power</li> <li>• needs stable base, needs 10-20 meter path</li> <li>• application above tall vegetation not possible yet</li> </ul>	<ul style="list-style-type: none"> <li>• can be operated on battery or solar power</li> <li>• relatively small, mast-mountable</li> <li>• remote sites and forests possible</li> </ul>
<b>Performance on concentration measurements</b>	<ul style="list-style-type: none"> <li>• operational in Dutch air quality monitoring network</li> <li>• traceable to certified standard within 3%</li> </ul>	<ul style="list-style-type: none"> <li>• substantial deviations, correlated to ambient temperature</li> </ul>
<b>Performance on flux measurements</b>	<ul style="list-style-type: none"> <li>• no golden standard available, instruments compare well, with exceptions</li> <li>• nighttime deposition fluxes similar, miniDOAS observes higher emissions during daytime</li> <li>• both need ~100 meter homogeneous, obstacle-free upwind terrain</li> <li>• both need further work on analysis algorithms</li> </ul>	
	<ul style="list-style-type: none"> <li>• footprint needs further study</li> </ul>	<ul style="list-style-type: none"> <li>• flux may or may not be affected by error in concentration measurement</li> </ul>

<sup>\*</sup> More details are given in <sup>1</sup> Sect. 1.4.1 and <sup>2</sup> Sect. 1.4.2. of the supplementary materials. <sup>3</sup> a more durable mirror is available now.

### 5.1 Concentration comparison

515 A substantial and varying discrepancy in NH<sub>3</sub> concentrations was found between the HT and the miniDOAS. The miniDOAS instrument is currently used for concentration monitoring in the Netherlands and has a validated accuracy of better than 3%. Therefore, we concluded that the observed discrepancy was caused by a substantial and varying offset in the HT concentrations, which correlated with the changing ambient air temperature (Figure S7,  $R^2 = 0.68$ ). Earlier, Wang et al. (2021) compared measured NH<sub>3</sub> concentrations of the HT to those of a Picarro instrument during a 14-h experimental period. The differences were within 10%. However, the indoor air temperature during that relatively short experiment would likely have been fairly stable, so any impact of temperature on HT concentration measurements could easily go undetected. Reliable measurements

of the absolute concentration are especially important for flux interpretation beyond the net flux, and also when calculating deposition velocities. It is therefore important to improve the accuracy of measured concentrations of the HT itself.

## 5.2 Flux comparison

525 The overall pattern of the fluxes and the diurnal cycles agreed remarkably well between the DOAS-AGM and the HT-EC setups when the wind came from the “green” sectors – where upwind terrain was relatively homogenous and obstacle-free. Larger differences were observed for the other wind directions (Figure 10). These discrepancies can have several causes.

530 First off, obstacles in the terrain upwind may interfere with both measurement techniques, as they affect atmospheric turbulence patterns and disturb the  $\text{NH}_3$  gradient. All instruments were influenced by the 213 m high tower (~ 60 m away), especially when the wind came from the southeast (red wind sector). Here, the correlation between the fluxes, however, was still modest ( $r = 0.69$ ). When the wind blew from the north (yellow wind sector), the agreement between AGM and EC fluxes was poorest ( $r = 0.33$ ). This may indicate that the heterogeneity of the footprint area had a larger influence on the fluxes measured by the two systems. Due to the differences in measurement height and path- versus point-sampling, the AGM and EC setups have different footprints (Loubet et al., 2013). If either the terrain or fluxes were inhomogeneous, the setups may therefore have  
535 captured different  $\text{NH}_3$  fluxes. At this site, spatial homogeneity may partly be violated by the ditches in the terrain. Direct emissions may be spatially inhomogeneous due to manure or fertiliser application or excreta from grazing animals. In a follow-up campaign, the comparison of the miniDOAS and the HT instrument should be continued at more homogeneous sites, avoiding nearby obstacles and (animal) emission sources within the footprints.

540 The substantial deviations in  $\text{NH}_3$  concentrations from the HT were strongly linked to ambient temperature. In the current analysis, we treated these deviations as a temperature-dependent offset. As ambient temperatures only changed gradually in time, so did the applied offset in the correction. As a consequence, this correction had virtually no impact on the HT flux measurement, as the flux measurement is based on observed concentration variations on a short timescale. It is however not clear if the effect of temperature is limited to inducing just an offset in concentration. There could also be an influence on the span: at higher temperatures the HT might be more, or less, sensitive to  $\text{NH}_3$ . This would affect the flux measurement by the  
545 same factor and could be an explanation for the discrepancy in flux between miniDOAS and HT during daytime (Figure 11). To eliminate this possible source of discrepancy, further studies to the cause and the exact effect of the temperature on the offset and slope of the HT calibration are necessary.

In this paper, standard flux processing was used for both techniques. Our instrument setups, however, are different from regular AGM and EC instruments (path versus point for miniDOAS, larger measurement volume for HT) and we are dealing with a  
550 new gas. These analysis techniques may therefore need adaptations. For example, we tested different damping methods and found different flux results. The theoretical damping correction (TEO) of Moncrieff et al. (1997) adds about 40% to the raw flux. When using the empirical (ICO) method (Wintjen et al., 2020) however, the damping effect was estimated to be only 30%. Since we do not have a very large dataset and because the empirical method can only properly run on the subset of the data that has fluxes large enough to make a reasonable spectral distribution, the fit of miniDOAS vs. HT when using ICO  
555 shows more scatter (Figure S13). We therefore choose to present the comparison based on the TEO correction, a method that is always available since it relies only on the arrangement and dimensions of the instrument. However, we strongly advise further evaluation of the damping calculation method. Similar advice is given for the AGM method, where we used the standard stability correction functions which bring a generalisation that might be not fully representative at our measurement site.

We compared two novel open-path optical instruments to measure  $\text{NH}_3$  concentration and flux during a 5-week comparison period at Cabauw, the Netherlands: two active custom-designed broadband UV-based miniDOAS (Differential Optical Absorption Spectroscopy) instruments and a commercially available infrared-based quantum cascade laser HT8700E gas analyser developed by the company Healthy Photon (HT). Both instruments avoid the hysteresis effects caused by the stickiness of  $\text{NH}_3$  to tubing and instrument interiors, and are as such insensitive to interference by ammonium aerosols. Both instruments showed good uptime during the campaign. The uptime of the miniDOAS system reached 100% once operational, but regular intercalibration of the two instruments was applied to test baseline stability (35% of the 7-week uptime). Intercalibration time can be reduced in future application based on the results of this campaign. The HT does not measure during rain, or shortly after rain while the instrument is drying, causing 21% data loss over the 5-week campaign. In addition, the coating of HT mirrors tended to degrade substantially.

The miniDOAS system measured fluxes using the aerodynamic gradient method (AGM), the HT8700E measured fluxes using the eddy covariance (EC) method. After data quality filtering, a total of 848 simultaneous half-hourly flux measurements were compared, showing that both instruments gave similar values for the  $\text{NH}_3$  exchange ranging from *ca.* -80 to +140  $\text{ng NH}_3 \text{ m}^{-2} \text{ s}^{-1}$  (Figure 10). When the upwind terrain was both homogenous and free of nearby obstacles within around 100 m, the two systems showed the strongest correlation ( $n = 113$ ,  $r = 0.87$ ) and provided similar temporal patterns. In addition, the observed diurnal pattern of the two systems had the same shape (Figure 11). As such, the deposition flux during night-time was *ca.* 25  $\text{ng NH}_3 \text{ m}^{-2} \text{ s}^{-1}$  (equivalent to 465  $\text{mol NH}_3 \text{ ha}^{-1} \text{ yr}^{-1}$ ). The highest emission occurred around noon and was up to 50  $\text{ng NH}_3 \text{ m}^{-2} \text{ s}^{-1}$ . Moreover, the AGM flux values were larger than the EC ones during daytime.

The uncertainty analysis showed that the random error of the two systems was similar (Figure 12). The median relative random errors were 23% for the AGM flux versus 15% for the EC flux. The median random error ( $1\sigma$ ) for half-hourly flux values of the miniDOAS was about 7.4  $\text{ng NH}_3 \text{ m}^{-2} \text{ s}^{-1}$ , and its maximum value generally did not exceed 15  $\text{ng m}^{-2} \text{ s}^{-1}$ . For the HT, the median and maximum random errors were 4.1 and 10  $\text{ng NH}_3 \text{ m}^{-2} \text{ s}^{-1}$ , respectively. These values are adequate to allow the study of deposition and emission processes. The random errors of both techniques varied substantially with meteorological conditions and time-of-day. For AGM flux, it was relatively higher during daytime. The diurnal cycle in the random error of the EC was, on the other hand, far less distinct.

While flux measurements between HT and miniDOAS in general compared well, we found a substantial variable offset in the HT concentrations. They were sensitive to air temperature, causing substantial differences (range: -15 to +6  $\mu\text{g m}^{-3}$ ) between the two systems. In this study, we used the miniDOAS as a reference to correct the HT concentration using a temperature-dependent offset and assuming no impact on the span. It should be stressed that these offset corrections only have an impact on the HT concentrations, not (or only very minor) on the HT fluxes. However, a temperature dependency in the span would also affect the HT fluxes. Further studies into the temperature dependence of the HT concentrations are needed to confirm the span calibration is indeed not impacted by changes in temperature.

The footprint analysis for the EC method showed that measurements were representative of the terrain up to approximately 100 m upwind. In the southeast direction, the footprint size was much smaller due to the meteorological measurement tower, which largely blocked the air flow. The footprint size of the AGM was not analysed but is expected to have a similar shape. Moreover, because of the lower measurement heights, the miniDOAS system is expected to have a smaller footprint, and the footprints of upper and lower paths are substantially different.

Spatial heterogeneous flux patterns need to be avoided in the upwind footprint region as they can influence the result and render interpretation more complicated or even impossible. Also, the 10% difference found between the theoretical (Moncrieff et al., 1997) and empirical (Wintjen et al., 2020) method for correcting high-frequency losses of EC fluxes may be related to inhomogeneities in the footprint area since they were not reproduced by theoretical cospectra. In addition, the terrain within all footprints needs to be homogeneous in its vegetation type and roughness. For further intercomparisons, obstacle-free, cattle-free, more homogeneous surroundings are highly recommended.

In deposition studies and parametrisations, reliable concentration and flux values are both needed. The miniDOAS provides both values reliably and appeared ready for long-term hands-off monitoring. The HT is presented solely as a flux instrument, and makes no claim to being an accurate monitor for NH<sub>3</sub> concentrations yet. In addition, the current system had a limited stand-alone operational time under the prevailing weather conditions.

In this study, we demonstrated that the miniDOAS and HT8700 systems provide comparable flux measurements at half-hourly time resolution. Under the right circumstances, data from both instruments can facilitate the study of processes behind dry deposition in different ecosystems, allowing better understanding and better parametrization of these processes in chemical transport models. These observations also enable to test and validate low-cost deposition measurement systems like the conditional time-averaged gradient (COTAG; Famulari et al., 2010), or inferential deposition networks (e.g. those listed by Walker et al., 2020).

## 7 Data availability

The datasets used in this study are available from the corresponding author upon request (susanna.jonker@rivm.nl, shelley.van.der.graaf@rivm.nl).

## 8 Author contribution

DS, AH, SR and TvG designed the study. DS and AH coordinated the field campaign. DS, SB, RvdH and MH developed and tested the miniDOAS instruments and performed measurements during the campaign. JZ, AH, AF and PvdB performed the EC HT measurements. JZ and PW processed the EC and HT data and determined the EC NH<sub>3</sub> flux. SB processed miniDOAS concentration data, and SvdG determined the AGM NH<sub>3</sub> flux. Figures were made by SvdG, SB and JZ. DS, AH and SR prepared the manuscript with contributions from JZ, SvdG, and SB. MvZ, RS, PW and TvG reviewed and corrected the draft manuscript.

## 9 Competing interests

The authors declare that they have no conflict of interest.

## 10 Acknowledgements

This work was done partly in the framework of the Dutch Ruisdael program (<https://ruisdael-observatory.nl>) and was part of the annual Ruisdael campaign (RITA-2021). Funding from the Ministry of Agriculture, Nature and Food Quality (LNV) is gratefully acknowledged. We thank the Royal Netherlands Meteorological Institute (KNMI) for site access and assistance during the campaign, especially Arnoud Apituley for coordination and help with site selection. We thank Dr. Kai Wang, from Institute of Atmospheric Physics, Chinese Academy of Sciences, Beijing; and staff from Healthy Photon Lt. Co, especially Dr.

Yin Wang and Dr. Peng Kang, for helpful discussions about data processing of the HT. Furthermore, we thank Daniëlle van  
640 Dinther (TNO) for merging various data streams during the campaign. We acknowledge RIVM colleagues Kim Vendel for  
the preliminary processing of the AGM data at beginning of the campaign, and Miranda Braam for helping with the uncertainty  
analysis.

## 11 References

- Bai, M., Suter, H., Macdonald, B., and Schwenke, G.: Ammonia, methane and nitrous oxide emissions from furrow irrigated  
645 cotton crops from two nitrogen fertilisers and application methods, *Agricultural and Forest Meteorology*, 303, 108375,  
<https://doi.org/10.1016/j.agrformet.2021.108375>, 2021.
- Bai, M., Loh, Z., Griffith, D. W. T., Turner, D., Eckard, R., Edis, R., Denmead, O. T., Bryant, G. W., Paton-Walsh, C., Tonini,  
M., McGinn, S. M., and Chen, D.: Performance of open-path lasers and FTIR spectroscopic systems in agriculture emissions  
research, *Atmos. Meas. Tech. Discuss.*, 2022, 1-18, 10.5194/amt-2021-347, 2022.
- 650 Beljaars, A. C. M. and Holtslag, A. A. M.: Flux parameterization over land surfaces for atmospheric models, *Journal of Applied  
Meteorology*, 30, 327-341, [https://www.doi.org/10.1175/1520-0450\(1991\)030<0327:Fpolsf>2.0.Co;2](https://www.doi.org/10.1175/1520-0450(1991)030<0327:Fpolsf>2.0.Co;2), 1991.
- Berkhout, A. J. C., Swart, D. P. J., Volten, H., Gast, L. F. L., Haaima, M., Verboom, H., Stefess, G., Hafkenscheid, T., and  
Hoogerbrugge, R.: Replacing the AMOR with the miniDOAS in the ammonia monitoring network in the Netherlands,  
*Atmospheric Measurement Techniques*, 10, 4099-4120, 10.5194/amt-10-4099-2017, 2017.
- 655 Bosveld, F. C.: The Cabauw in-situ observational program 2000 - present: instruments, calibrations and set-up, Royal  
Netherlands Meteorological Institute, De Bilt, 2020.
- Bosveld, F. C., Baas, P., Beljaars, A. C. M., Holtslag, A. A. M., de Arellano, J. V.-G., and van de Wiel, B. J. H.: Fifty years  
of atmospheric boundary-layer research at Cabauw serving weather, air quality and climate, *Boundary-Layer Meteorology*,  
177, 583-612, 10.1007/s10546-020-00541-w, 2020.
- 660 Burba, G., Anderson, T., and Komissarov, A.: Accounting for spectroscopic effects in laser-based open-path eddy covariance  
flux measurements, *Global Change Biology*, 25, 2189-2202, <https://doi.org/10.1111/gcb.14614>, 2019.
- Dyer, A. J.: A review of flux-profile relationships, *Boundary-Layer Meteorology*, 7, 363-372,  
<https://www.doi.org/10.1007/BF00240838>, 1974.
- 665 Erisman, J. W. and Wyers, G. P.: Continuous measurements of surface exchange of SO<sub>2</sub> and NH<sub>3</sub>; Implications for their  
possible interaction in the deposition process, *Atmospheric Environment. Part A. General Topics*, 27, 1937-1949,  
[https://doi.org/10.1016/0960-1686\(93\)90266-2](https://doi.org/10.1016/0960-1686(93)90266-2), 1993.
- Erisman, J. W., Galloway, J. N., Dice, N. B., Sutton, M. A., Bleeker, A., Grizzetti, B., Leach, A. M., and Vries, W. d.: Nitrogen:  
too much of a vital resource, *Science Brief. WWF Netherlands, Zeist, The Netherlands*, 2015.
- 670 Famulari, D., Fowler, D., Hargreaves, K., Milford, C., Nemitz, E., Sutton, M. A., and Weston, K.: Measuring eddy covariance  
fluxes of ammonia using tunable diode laser absorption spectroscopy, *J Water, Air, Soil Pollution: Focus*, 4, 151-158,  
10.1007/s11267-005-3025-9, 2004.
- Famulari, D., Fowler, D., Nemitz, E., Hargreaves, K. J., Storeton-West, R. L., Rutherford, G., Tang, Y. S., Sutton, M. A., and  
Weston, K. J.: Development of a low-cost system for measuring conditional time-averaged gradients of SO<sub>2</sub> and NH<sub>3</sub>,  
*Environmental Monitoring Assessment*, 161, 11-27, 10.1007/s10661-008-0723-6, 2010.
- 675 Flechard, C. R., Nemitz, E., Smith, R. I., Fowler, D., Vermeulen, A. T., Bleeker, A., Erisman, J. W., Simpson, D., Zhang, L.,  
Tang, Y. S., and Sutton, M. A.: Dry deposition of reactive nitrogen to European ecosystems: a comparison of inferential models  
across the NitroEurope network, *Atmospheric Chemistry and Physics*, 11, 2703-2728, <https://www.doi.org/10.5194/acp-11-2703-2011>, 2011.
- Flesch, T. K., Baron, V. S., Wilson, J. D., Griffith, D. W. T., Basarab, J. A., and Carlson, P. J.: Agricultural gas emissions  
680 during the spring thaw: Applying a new measurement technique, *Agricultural and Forest Meteorology*, 221, 111-121,  
<https://doi.org/10.1016/j.agrformet.2016.02.010>, 2016.
- Foken, T.: *Micrometeorology*, Springer Berlin Heidelberg, 384 pp.2017.
- Fowler, D., Coyle, M., Skiba, U., Sutton, M. A., Cape, J. N., Reis, S., Sheppard, L. J., Jenkins, A., Grizzetti, B., Galloway, J.  
N., Vitousek, P., Leach, A., Bouwman, A. F., Butterbach-Bahl, K., Dentener, F., Stevenson, D., Amann, M., and Voss, M.:  
685 The global nitrogen cycle in the twenty-first century, *Philosophical Transactions of the Royal Society B: Biological Sciences*,  
368, 20130164, 10.1098/rstb.2013.0164, 2013.
- Galloway, J. N., Bleeker, A., and Erisman, J. W.: The human creation and use of reactive nitrogen: a global and regional  
perspective, *Annual Review of Environment and Resources*, 46, 255-288, 10.1146/annurev-environ-012420-045120, 2021.
- Homan, C.: *Maandoverzicht van het weer in Nederland*, September 2021, KNMI, De Bilt, 2021.
- 690 Hoogerbrugge, R., Geilenkirchen, G. P., Hollander, H. A. d., Schuch, W., Swaluw, E. v. d., Vries, W. J. d., and Kruit, R. J.  
W.: Grootschalige concentratie- en depositiekaarten Nederland - Rapportage 2020, Rijksinstituut voor Volksgezondheid en  
Milieu, Bilthoven, 2020.
- Jager, C. J., Nakken, T. C., and Palland, C. L.: *Bodemkundig onderzoek van twee graslandpercelen nabij Cabauw.*, Arnhem  
(In Dutch), 1976.
- 695 Kaimal, J. C., Wyngaard, J. C., Izumi, Y., and Coté, O. R.: Spectral characteristics of surface-layer turbulence, *Quarterly  
Journal of the Royal Meteorological Society*, 98, 563-589, <https://doi.org/10.1002/qj.49709841707>, 1972.

- Kamp, J. N., Häni, C., Nyord, T., Feilberg, A., and Sørensen, L. L.: The aerodynamic gradient method: implications of non-simultaneous measurements at alternating heights, *Atmosphere*, 11, 1067, 2020.
- 700 Kljun, N., Calanca, P., Rotach, M. W., and Schmid, H. P.: A simple two-dimensional parameterisation for Flux Footprint Prediction (FFP), *Geosci. Model Dev.*, 8, 3695-3713, 10.5194/gmd-8-3695-2015, 2015.
- Loubet, B. and Personne, E.: Application note 28 - Measuring emissions from diffuse sources using the aerodynamic gradient, in: *Measuring emissions from livestock farming: greenhouse gases, ammonia and nitrogen oxides*, edited by: Hassouna, M., Eglin, T., Cellier, P., Colomb, V., Cohan, J.-P., Decuq, C., Delabuis, M., Edouard, N., Espagnol, S., Eugène, M., Fauvel, Y., Fernandes, E., Fischer, N., Flechard, C., Genermont, S., Godbout, S., Guingand, N., Guyader, J., Lagadec, S., Laville, P.,
- 705 Lorinquer, E., Loubet, B., Loyon, L., Martin, C., Méda, B., Morvan, T., Oster, D., Oudart, D., Personne, E., Planchais, J., Ponchant, P., Renand, G., Robin, P., and Rochette, Y., INRA-ADEME, np, 2016.
- Loubet, B., Decuq, C., Personne, E., Massad, R. S., Flechard, C., Fanucci, O., Mascher, N., Gueudet, J. C., Masson, S., Durand, B., Genermont, S., Fauvel, Y., and Cellier, P.: Investigating the stomatal, cuticular and soil ammonia fluxes over a growing triticale crop under high acidic loads, *Biogeosciences*, 9, 1537-1552, 10.5194/bg-9-1537-2012, 2012.
- 710 Loubet, B., Cellier, P., Fléchar, C., Zurfluh, O., Irvine, M., Lamaud, E., Stella, P., Roche, R., Durand, B., Flura, D., Masson, S., Laville, P., Garrigou, D., Personne, E., Chelle, M., and Castell, J.-F.: Investigating discrepancies in heat, CO<sub>2</sub> fluxes and O<sub>3</sub> deposition velocity over maize as measured by the eddy-covariance and the aerodynamic gradient methods, *Agricultural and Forest Meteorology*, 169, 35-50, <https://doi.org/10.1016/j.agrformet.2012.09.010>, 2013.
- Mauder, M. and Foken, T.: Impact of post-field data processing on eddy covariance flux estimates and energy balance closure
- 715 *Meteorologische Zeitschrift*, 15, 597-609, <https://doi.org/10.1127/0941-2948/2006/0167>, 2006.
- Mauder, M., Foken, T., Aubinet, M., and Ibrom, A.: Eddy-covariance measurements, in: *Springer Handbook of Atmospheric Measurements*, edited by: Foken, T., Springer International Publishing, Cham, 1485-1515, 10.1007/978-3-030-52171-4\_55, 2021.
- McDermitt, D. K., Burba, G., Xu, L., Anderson, T. G., Komissarov, A. V., Riensche, B., Schedlbauer, J. L., Starr, G., Zona, D., Oechel, W. C., Oberbauer, S. F., and Hastings, S. J.: A new low-power, open-path instrument for measuring methane flux by eddy covariance, *Applied Physics B*, 102, 391-405, doi:10.1007/s00340-010-4307-0, 2011.
- 720 Miller, D. J., Sun, K., Tao, L., Khan, M. A., and Zondlo, M. A.: Open-path, quantum cascade-laser-based sensor for high-resolution atmospheric ammonia measurements, *Atmos. Meas. Tech.*, 7, 81-93, 10.5194/amt-7-81-2014, 2014.
- Moncrieff, J., Clement, R., Finnigan, J., Meyers, T., Lee, X., Massman, W., and Law, B.: Averaging, detrending, and filtering of eddy covariance time series, in: *Handbook of micrometeorology; A guide for surface flux measurement and analysis*, edited by: Lee, X., Massman, W., and Law, B., Atmospheric and oceanographic sciences library, Kluwer Academic Publisher, Dordrecht, The Netherlands, 7-32, 2004.
- 725 Moncrieff, J. B., Massheder, J. M., de Bruin, H., Elbers, J., Friborg, T., Heusinkveld, B., Kabat, P., Scott, S., Soegaard, H., and Verhoef, A.: A system to measure surface fluxes of momentum, sensible heat, water vapour and carbon dioxide, *Journal of Hydrology*, 188-189, 589-611, [https://doi.org/10.1016/S0022-1694\(96\)03194-0](https://doi.org/10.1016/S0022-1694(96)03194-0), 1997.
- 730 Moore, C. J.: Frequency response corrections for eddy correlation systems, *Boundary-Layer Meteorology*, 37, 17-35, 10.1007/BF00122754, 1986.
- Moravek, A., Singh, S., Pattey, E., Pelletier, L., and Murphy, J. G.: Measurements and quality control of ammonia eddy covariance fluxes: a new strategy for high-frequency attenuation correction, *Atmos. Meas. Tech.*, 12, 6059-6078, 10.5194/amt-12-6059-2019, 2019.
- 735 Pan, D., Benedict, K. B., Golston, L. M., Wang, R., Collett, J. L., Tao, L., Sun, K., Guo, X., Ham, J., Prenni, A. J., Schichtel, B. A., Mikoviny, T., Müller, M., Wisthaler, A., and Zondlo, M. A.: Ammonia dry deposition in an alpine ecosystem traced to agricultural emission hotspots, *Environmental Science & Technology*, 55, 7776-7785, 10.1021/acs.est.0c05749, 2021.
- Parrish, D. D. and Fehsenfeld, F. C.: Methods for gas-phase measurements of ozone, ozone precursors and aerosol precursors, *Atmospheric Environment*, 34, 1921-1957, [https://doi.org/10.1016/S1352-2310\(99\)00454-9](https://doi.org/10.1016/S1352-2310(99)00454-9), 2000.
- 740 Paulson, C. A.: The mathematical representation of wind speed and temperature profiles in the unstable atmospheric surface layer, *Journal of Applied Meteorology*, 9, 857-861, [https://www.doi.org/10.1175/1520-0450\(1970\)009<0857:Tmrows>2.0.Co;2](https://www.doi.org/10.1175/1520-0450(1970)009<0857:Tmrows>2.0.Co;2), 1970.
- Platt, U. and Stutz, J.: *Differential Optical Absorption Spectroscopy - Principles and Applications*, Springer, Berlin 2008.
- 745 Prueger, J. H. and Kustas, W. P.: Aerodynamic methods for estimating turbulent fluxes in: *Micrometeorology in Agricultural Systems*, American Society of Agronomy, Crop Science Society of America, Soil Science Society of America, Madison, 2005.
- Schulte, R. B., van Zanten, M. C., Rutledge-Jonker, S., Swart, D. P. J., Wichink Kruit, R. J., Krol, M. C., van Pul, W. A. J., and Vilà-Guerau de Arellano, J.: Unraveling the diurnal atmospheric ammonia budget of a prototypical convective boundary layer, *Atmospheric Environment*, 118153, <https://doi.org/10.1016/j.atmosenv.2020.118153>, 2020.
- 750 Sintermann, J., Dietrich, K., Häni, C., Bell, M., Jocher, M., and Neftel, A.: A miniDOAS instrument optimised for ammonia field measurements, *Atmospheric Measurement Techniques*, 9, 2721-2734, 10.5194/amt-9-2721-2016, 2016.
- Sintermann, J., Ammann, C., Kuhn, U., Spirig, C., Hirschberger, R., G'artner, A., and Neftel, A.: Determination of field scale ammonia emissions for common slurry spreading practice with two independent methods, *Atmospheric Measurement Techniques*, 4, 1821-1840, 2011.
- 755 Sun, K., Tao, L., Miller, D. J., Zondlo, M. A., Shonkwiler, K. B., Nash, C., and Ham, J. M.: Open-path eddy covariance measurements of ammonia fluxes from a beef cattle feedlot, *Agricultural and Forest Meteorology*, 213, 193-202, <http://dx.doi.org/10.1016/j.agrformet.2015.06.007>, 2015.
- Sutton, M. A., Oenema, O., Erisman, J. W., Leip, A., van Grinsven, H., and Winiwarter, W.: Too much of a good thing, *Nature*, 472, 159-161, 10.1038/472159a, 2011.

- 760 Trebs, I., Ammann, C., and Junk, J.: Immission and dry deposition, in: Springer Handbook of Atmospheric Measurements, edited by: Foken, T., Springer Handbooks, Springer, Cham., [https://doi.org/10.1007/978-3-030-52171-4\\_54](https://doi.org/10.1007/978-3-030-52171-4_54), 2021.
- Volten, H., Haaima, M., Swart, D., van Zanten, M., and van Pul, W.: Ammonia exchange measured over a corn field in 2010, National Institute of Public Health and the Environment, Bilthoven, The Netherlands, 2012a.
- Volten, H., Bergwerff, J. B., Haaima, M., Lolkema, D. E., Berkhout, A. J. C., van der Hoff, G. R., Potma, C. J. M., Wichink Kruit, R. J., van Pul, W. A. J., and Swart, D. P. J.: Two instruments based on differential optical absorption spectroscopy (DOAS) to measure accurate ammonia concentrations in the atmosphere, *Atmospheric Measurement Techniques*, 5, 413-427, <https://www.doi.org/10.5194/amt-5-413-2012>, 2012b.
- Walker, J. T., Beachley, G., Zhang, L., Benedict, K. B., Sive, B. C., and Schwede, D. B.: A review of measurements of air-surface exchange of reactive nitrogen in natural ecosystems across North America, *Science of The Total Environment*, 698, 133975, <https://doi.org/10.1016/j.scitotenv.2019.133975>, 2020.
- Walker, J. T., Jones, M. R., Bash, J. O., Myles, L., Meyers, T., Schwede, D., Herrick, J., Nemitz, E., and Robarge, W.: Processes of ammonia air-surface exchange in a fertilized *Zea mays* canopy, *Biogeosciences*, 10, 981-998, 10.5194/bg-10-981-2013, 2013.
- Wang, K., Kang, P., Lu, Y., Zheng, X., Liu, M., Lin, T.-J., Butterbach-Bahl, K., and Wang, Y.: An open-path ammonia analyzer for eddy covariance flux measurement, *Agricultural and Forest Meteorology*, 308-309, 108570, <https://doi.org/10.1016/j.agrformet.2021.108570>, 2021.
- Wang, K., Wang, J., Qu, Z., Xu, W., Wang, K., Zhang, H., Shen, J., Kang, P., Zhen, X., Wang, Y., Zheng, X., and Liu, X.: A significant diurnal pattern of ammonia dry deposition to a cropland is detected by an open-path quantum cascade laser-based eddy covariance instrument, *Atmospheric Environment*, <https://doi.org/10.1016/j.atmosenv.2022.119070>, 2022.
- 780 Webb, E. K., Pearman, G. I., and Leuning, R.: Correction of flux measurements for density effects due to heat and water vapour transfer, *Quarterly Journal of the Royal Meteorological Society*, 106, 85-100, <https://doi.org/10.1002/qj.49710644707>, 1980.
- Wichink Kruit, R. J., H, V., M, H., DPJ, S., MC, v. Z., and WAJ, v. P.: Ammonia exchange measurements over a corn field in Lelystad, the Netherlands in 2009, National Institute for Public Health and the Environment, Bilthoven, The Netherlands, 2010.
- 785 Wintjen, P., Ammann, C., Schrader, F., and Brümmer, C.: Correcting high-frequency losses of reactive nitrogen flux measurements, *Atmos. Meas. Tech.*, 13, 2923-2948, 10.5194/amt-13-2923-2020, 2020.
- Wolff, V., Trebs, I., Ammann, C., and Meixner, F. X.: Aerodynamic gradient measurements of the NH<sub>3</sub>-HNO<sub>3</sub>-NH<sub>4</sub>NO<sub>3</sub> triad using a wet chemical instrument: an analysis of precision requirements and flux errors, *Atmos. Meas. Tech.*, 3, 187-208, <https://www.doi.org/10.5194/amt-3-187-2010>, 2010.
- 790 Zöll, U., Brümmer, C., Schrader, F., Ammann, C., Ibrom, A., Flechard, C. R., Nelson, D. D., Zahniser, M., and Kutsch, W. L.: Surface-atmosphere exchange of ammonia over peatland using QCL-based eddy-covariance measurements and inferential modeling, *Atmospheric Chemistry and Physics*, 16, 11283-11299, 10.5194/acp-16-11283-2016, 2016.